Towards the complete phase profiling of attosecond wave packets

Jaco Fuchs,[1,*] Nicolas Douguet,[2,3] Stefan Donsa,[4] Fernando Martín,[5,6,7] Joachim Burgdörfer,[4] Luca Argenti,[3,8] Laura Cattaneo,[1] and Ursula Keller[1]

[1]*Department of Physics, ETH Zürich, Zürich, Switzerland*
[2]*Department of Physics, Kennesaw State University, Marietta, Georgia, USA*
[3]*Department of Physics, University of Central Florida, Orlando, Florida, USA*
[4]*Institute of Theoretical Physics, Vienna University of Technology, Vienna, Austria, European Union*
[5]*Departamento de Química Modulo 13, Universidad Autónoma de Madrid, 28049 Madrid, Spain, European Union*
[6]*Condensed Matter Physics Center (IFIMAC), Universidad Autonoma de Madrid, 28049 Madrid, Spain, European Union*
[7]*Instituto Madrileño de Estudios Avanzados en Nanociencia (IMDEA-Nano), 28049 Madrid, Spain, European Union*
[8]*CREOL, University of Central Florida, Orlando, Florida 32186, USA*

(Received 2 August 2020; revised 9 February 2021; accepted 9 February 2021; published 26 February 2021)

Realistic attosecond wave packets have complex profiles that, in dispersive conditions, rapidly broaden or split in multiple components. Such behaviors are encoded in sharp features of the wave packet spectral phase. Here we exploit the quantum beating between one- and two-photon transitions in an attosecond photoionization experiment to measure the photoelectron spectral phase continuously across a broad energy range. Supported by numerical simulations, we demonstrate that this experimental technique is able to reconstruct sharp fine-scale features of the spectral phase, continuously as a function of energy and across the full spectral range of an attosecond pulse train. In a proof-of-principle experiment, we observe the periodic modulations of the spectral phase of an attosecond pulse train due to the individual chirp of each harmonic.

DOI: 10.1103/PhysRevResearch.3.013195

I. INTRODUCTION

Attosecond photoionization time delays provide a precise timing of electronic motion in atoms [1–3], molecules [4,5], and solids [6–9]. Defined as group delay difference between two electron wave packets, they set benchmarks for the most advanced quantum simulations [10–12]. However, as group delays are given by the first-order expansion of the spectral phase $\varphi(E)$, they cannot characterize the full wave packet evolution. Indeed, dynamical aspects more complex than a simple delay, such as changes in the wave packet envelope shape, can only be reconstructed if the energy-dependent spectral phase is measured in full. In particular, strong and sharp variations of $\varphi(E)$ are key to the most intricate wave packet dynamics [3,13–16].

Most experimental techniques currently used to characterize photoionization phases can retrieve only the average value of the group delay across a broad energy range, e.g., the whole attosecond pulse bandwidth in streaking measurements [1,17,18], or at discrete energies spaced by twice the probe frequency, in the RABBITT (reconstruction of attosecond beatings by interference of two-photon transitions) scheme [19,20]. In these techniques, therefore, rapid phase variations with energy are typically lost. A few techniques to retrieve full phase profiles in streaking measurements using pulse reconstruction algorithms have been proposed [21,22], some of which are, in principle, also applicable to pulse trains [21]. Similarly, a few interferometric schemes have been proposed to resolve sharp spectral features: by dispersing broad RABBITT sidebands [3,13,23], by scanning the probe frequency across the feature [14,24], or by employing bicircular attosecond pulse trains [25]. Even these more advanced schemes, however, are sensitive only to the difference of the spectral phase between two isolated harmonics, and hence they can characterize the wave packet profile in more detail only under the *ad hoc* assumption that the harmonics are Fourier limited. The question arises, therefore, whether sharp phase variations associated with either the impinging light or the electronic structure of the target can be directly observed.

In this work, we demonstrate that the quantum beat between one- and two-photon transitions, formerly referred to as 1-2 quantum beat [26–29], together with angle-resolved electron spectroscopy, provides direct access to complex structures in the spectral phase of the photoionized electron wave packets, which, to the best of our knowledge, are, otherwise, accessible only by complete pulse reconstruction techniques. In contrast to the previous methods [26–29], we enable the 1-2 quantum beat by performing a RABBITT-inspired experiment using an extreme ultraviolet (XUV) attosecond pulse train (APT) with only odd, but spectrally broad, high harmonics. The combination of the 1-2 quantum beat with spectrally broad high harmonics allows us to retrieve

*jafuchs@phys.ethz.ch

phase differences continuously as a function of energy and across the entire bandwidth of the XUV spectrum; i.e., it allows for a complete phase profiling. In a proof-of-principle experiment, we observe periodic oscillations in the phase of electron wave packets generated by photoionization from helium. Supported by numerical solutions of the time-dependent Schrödinger equation (TDSE), we can attribute these phase oscillations to the harmonic chirp of the XUV pulse train inherent to the underlying high harmonic generation (HHG) process. Whereas the harmonic chirp has been successfully quantified for single harmonics [30–35], direct observations of the underlying phase modulations across the full spectrum, originally predicted more than 15 years ago [36,37], are scarce [38].

II. METHOD

The spectral phase of a photoelectron wave packet created by absorption of one XUV photon comprises two contributions, the Eisenbud-Wigner-Smith (EWS) scattering phase due to half-scattering at the ionic potential [39,40] and the spectral phase of the ionizing light pulse. The spectral phase of photo-emitted electrons, therefore, can be used either to study the EWS scattering phase [41,42] or to characterize XUV light pulses [43,44].

Figure 1(a) illustrates the comparison between the RABBITT and the 1-2 quantum beat method described in this work. Upon XUV photoionization (pump) an IR pulse (probe) promotes continuum-continuum (cc) transitions [45,46]. As the pump-probe delay is varied, the photoelectron signal beats as a result of the interference between quantum pathways with the same final energy. The phase of this beating is directly linked to the spectral phase difference between the two interfering quantum paths. Whereas RABBITT is based on the interference between two different two-photon pathways, i.e., a 2-2 quantum beat [19,20], the 1-2 quantum beat [26–29] method exploits the interference between one-photon and two-photon pathways.

To illustrate the different sensitivity of the two approaches to sharp features in the spectral phase, we first consider an idealized ionization experiment for which we assume that in the energy regime of interest the atomic ionization cross section is constant and the EWS and cc-phases are negligible. Under these assumptions, the phase of the ionized electron wave packet directly reflects the phase of the XUV spectrum. The XUV spectrum [Fig. 1(b)] used in the calculation features a strong and well-localized spectral phase variation at its center that may mimic the effect of a complex high-harmonic generation process or the resonant ionization phase of the target. As can be seen in Figs. 1(c) and 1(e), RABBITT is blind to the sharp phase variation, while the 1-2 quantum beat is particularly sensitive to it [Figs. 1(d) and 1(f)]. The retrieved phase differences provide detailed information on the spectral phase $\varphi(E)$ well beyond its first derivative at the center, as we will show below.

The XUV-APT spectrum is composed of odd high harmonics of an IR laser field which result in mainbands (MBs) (one-photon transitions) in the photoelectron spectrum, separated by twice the IR photon energy $\hbar\omega_{\mathrm{IR}}$. Interaction with the IR probe leads to the appearance of sidebands (SB) between

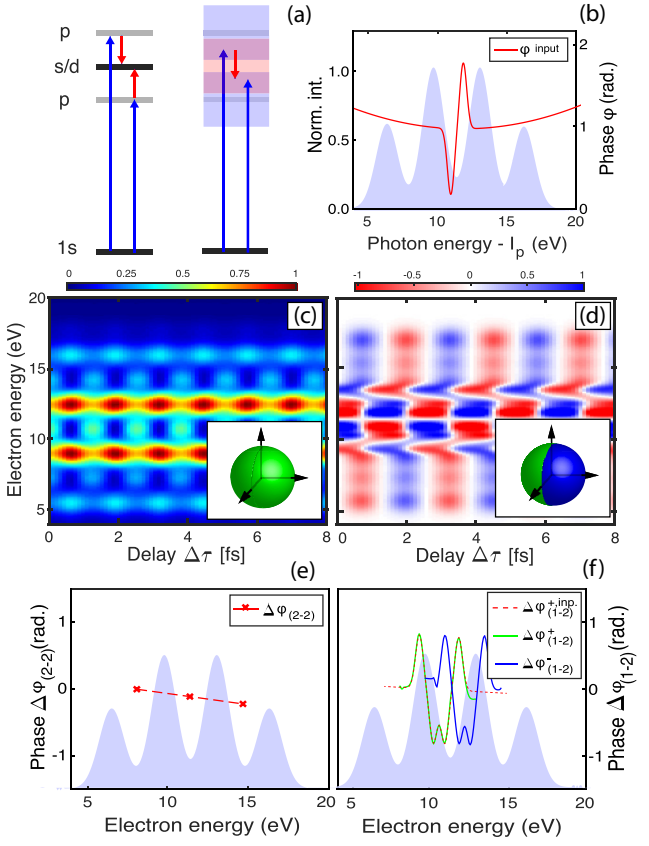

FIG. 1. (a) RABBITT (2-2 quantum beat) and the 1-2 quantum beat protocol, schematically. Blue arrows indicate photoionization induced by the XUV, and red arrows indicate cc-transitions induced by the IR. (b) Amplitude and phase of the input XUV pulse. (c) RABBITT trace (total yield). The inset indicates the integration over all emission angles. (d) Asymmetry trace extracted from the 1-2 quantum beat. The inset indicates the asymmetry of the angular distribution (difference left-right). (e) Phase difference $\Delta\varphi_{2-2}(E)$ extracted from the RABBITT sidebands. (f) Phase differences $\Delta\varphi^{+}_{1-2}(E)$ and $\Delta\varphi^{-}_{1-2}(E)$ extracted from the 1-2 quantum beat method and comparison with $\Delta\varphi^{+,\mathrm{inp.}}_{1-2}(E)$ from the input phase.

the MBs, whose intensities oscillate as a function of the pump-probe delay τ at twice the IR laser frequency $2\omega_{\mathrm{IR}}$ [Fig. 1(c)]. The beating is symmetric along the common light polarization axis as only partial waves with the same parity interfere. The phase offset of each sideband corresponds to the phase difference between the neighboring harmonics extracted by RABBITT $\Delta\varphi_{2-2} = \varphi(E + \hbar\omega_{\mathrm{IR}}) - \varphi(E - \hbar\omega_{\mathrm{IR}})$. Since this phase difference can be sampled only at the sideband positions, the sharply structured phase profile remains undetected [Fig. 1(e)], even though the XUV spectrum spans the entire energy region.

In the 1-2 quantum beat method, by contrast, the interference of partial waves with opposite parity ($s - p$ or $p - d$) gives rise to an asymmetry of the electron angular distribution that beats at the angular frequency ω_{IR} as a function of τ [Fig. 1(d)] [26,27]. This asymmetry, determined here by the difference of electron yield emitted to opposite sides of the plane perpendicular to the light polarization is shown in Fig. 1(d). For the ultrashort APT employed here, both two-

photon pathways (absorption and stimulated emission of an IR photon) can interfere with the one-photon amplitude across the whole spectral width of the APT. As long as the harmonics are spectrally sufficiently broad, therefore, the two phase differences $\Delta\varphi^{+}_{1-2}(E) = \varphi(E-\hbar\omega_{\mathrm{IR}}) - \varphi(E)$ and $\Delta\varphi^{-}_{1-2}(E) = \varphi(E) - \varphi(E+\hbar\omega_{\mathrm{IR}})$ can both be retrieved continuously as a function of energy and the sharp phase profile is detected. As we will show below, the two phase differences can be approximately retrieved fully analytically from the asymmetry trace. Furthermore, as the one-photon pathway is itself part of the interference, the retrieved phases are unaffected by the finite spectral bandwidth of the IR [23]. For sharp resonances (see, e.g., Fig. 1) the two-photon pathways serve as a flat reference, such that the retrieved phases remain sharp.

III. THEORETICAL FRAMEWORK

The angle-dependent ionization probability is [3]

$$I(E,\vartheta,\tau) = \left|\sum_{\ell}(A^{+}_{\ell} + A^{-}_{\ell})Y^{0}_{\ell}(\vartheta) + iA^{1}_{1}Y^{0}_{1}(\vartheta)\right|^{2}, \qquad (1)$$

where A^{1}_{1} and $A^{\pm}_{\ell}$ are the one-photon and two-photon amplitudes ($+/-$ designates IR absorption/emission, and $\ell = 0, 2$ is the photoelectron orbital angular momentum), Y^{m}_{ℓ} are spherical harmonics with $m = 0$ due to the collinear alignment of the employed light fields, and ϑ is the angle between the electron photoemission direction and the common light polarization axis. The energy-dependent ionization cross section is thereby included in A^{1}_{1}. The one- and two-photon amplitudes of the quantum pathways are functions of the kinetic energy E and of the pump-probe delay τ [45],

$$A^{1}_{1} = |A^{1}_{1}|e^{i\varphi(E)}, \quad A^{\pm}_{\ell} = |A^{\pm}_{\ell}|e^{i(\varphi^{\pm}_{\ell}(E)\pm\omega\tau)}. \qquad (2)$$

The spectral phase of the one-photon XUV ionization $\varphi(E) = \varphi^{1}_{\ell=1}(E)$ contains the EWS scattering phase and the XUV phase. The photoelectron asymmetry signal

$$f_a(E,\tau) = I(E,\tau)_{\vartheta\leqslant 90^{\circ}} - I(E,\tau)_{\vartheta\geqslant 90^{\circ}}, \qquad (3)$$

given by the difference between emission into the forward and backward hemispheres, then follows as

$$f_a(E,\tau) = \sum_{\sigma,\ell}\sigma c_{\ell}|A^{1}_{1}||A^{\sigma}_{\ell}| \times \sin\left\{\omega\tau + \sigma\left[\varphi^{\sigma}_{\ell}(E) - \varphi^{1}_{1}(E)\right]\right\}, \qquad (4)$$

where $\sigma = \pm$, $c_0 = \sqrt{3}$, and $c_2 = \sqrt{15}/4$. For a simplified analytic estimate, the two-photon pathways can be approximated by the one-photon phase as $\varphi^{\sigma}_{\ell}(E) \simeq \varphi^{1}_{1}(E - \sigma\hbar\omega_{\mathrm{IR}})$ since the method is sensitive only to phase variations but not to absolute phases. The cc-phase for different angular momenta [46] can be neglected since its variation is small within the present energy range. Likewise, the cc-transition probabilities to different ℓ are only weakly energy and ℓ dependent, such that $|A^{\sigma}_{\ell}| \approx |A^{\pm}|$ [47].

Consequently,

$$f_a(E,\tau) \simeq A(E)\sin[\omega\tau + \delta(E)], \qquad (5)$$

where $A(E)$ and $\delta(E)$ are the modulus and phase of $a^{+}e^{i\Delta\varphi^{+}_{1-2}} - a^{-}e^{i\Delta\varphi^{-}_{1-2}}$, with $a^{\sigma}(E) = |A^{1}_{1}||A^{\sigma}|(c_0 + c_2)$ and $\Delta\varphi^{\sigma}_{1-2}(E) = \sigma(\varphi(E - \sigma\hbar\omega_{\mathrm{IR}}) - \varphi(E))$. This approximate relationship [Eq. (5)] illustrates the sensitivity of the 1-2 quantum beat method to rapid variations of the spectral phase. For energy-independent phases, $A(E)$ vanishes, as $a^{+}(E) \approx a^{-}(E)$. By contrast, phase differences $\Delta\varphi^{\pm}$ that vary rapidly within $\hbar\omega_{IR}$ result in strong oscillations of the photoemission asymmetry. A similar expression is also obtained in the PROOF (Phase Retrieval by Omega Oscillation Filtering) method [22], based on the strong field approximation.

IV. EXPERIMENTAL RESULTS

Figure 2 shows the results of a proof-of-principle experiment performed with atomic helium. The experiment is carried out resembling the RABBITT protocol and using an XUV-APT with spectrally broad high harmonics. The XUV-APT is generated via HHG using a 10 fs FWHM IR laser pulse centered around 785 nm from a carrier-envelope-phase (CEP) stabilized Ti:sapphire laser system. In contrast to previous experiments, where the 1-2 quantum beat has been enabled by a combination of even and odd harmonics [26,27], the CEP stabilization is essential for the observation of the asymmetry signal in our experiment, where the 1-2-quantum beat is enabled by spectrally overlapping high harmonics. The XUV-APT is focused together with a collinear time-delayed replica of the generating IR pulse on a cold helium gas jet. The resulting photoelectrons are collected with a cold target recoil ion momentum spectrometer (COLTRIMS) [49], which allows for an angular resolved detection [50]. The setup is described in detail in Ref. [51]. In the delay-integrated RABBITT spectrum the MBs are depleted as compared to the

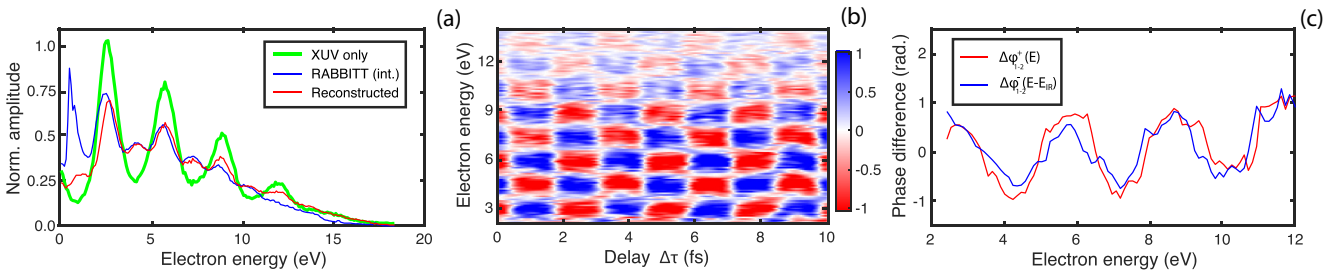

FIG. 2. (a) XUV-only (green) and delay-integrated RABBITT spectrum (blue) from the experiment. The red curve results from the fit of the transition ratios [Eq. (7)] to the integrated RABBITT spectrum in the range from 3 eV to 12 eV. (b) Measured asymmetry signal, defined as in Eq. (3), as a function of pump-probe delay. (c). Retrieved phases $\Delta\varphi^{+}_{1-2}(E)$ and $\Delta\varphi^{-}_{1-2}(E - \hbar\omega_{\mathrm{IR}})$ from the experiment.

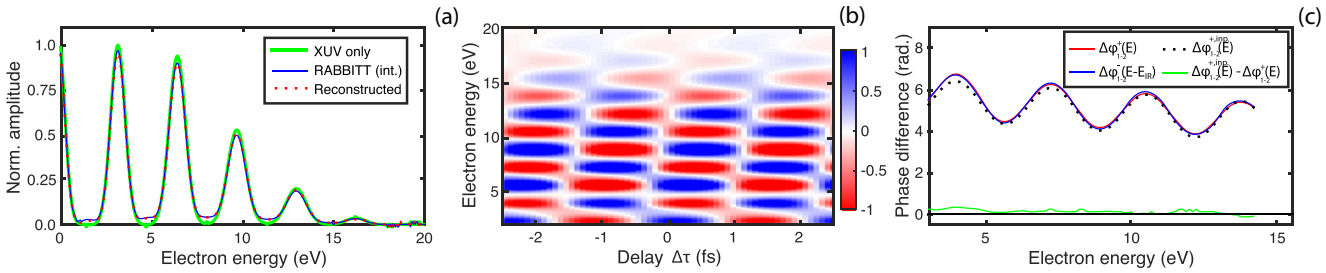

FIG. 3. (a) XUV-only (green) and delay-integrated RABBITT spectrum (blue) from the quantum simulation employing a single-active electron (SAE) approximation and a model potential from Ref. [48]. The red curve results from a fit of the transition ratios [Eq. (7)] to the integrated RABBITT spectrum in the range from 2 eV to 14 eV. (b) Calculated asymmetry signal, defined as in Eq. (3), as a function of pump-probe delay. (c) Retrieved phases $\Delta\varphi^{+}_{1-2}(E)$ (red) and $\Delta\varphi^{-}_{1-2}(E-\hbar\omega_{\mathrm{IR}})$ (blue) in comparison to $\Delta\varphi^{+,inp.}_{1-2}(E)$ from the input phase. The difference between the retrieved phase $\Delta\varphi^{+}_{1-2}(E)$ and the input phase $\Delta\varphi^{+,inp.}_{1-2}(E)$ is shown explicitly (green).

XUV-only spectrum due to the IR induced cc-transitions to the SBs [Fig. 2(a)]. The asymmetry shows a checkerboard pattern [Fig. 2(b)], which implies an energy dependence of the spectral phase. If the phase were spectrally flat, only a weak and constant asymmetry signal comparable to the upper (or lower) part in Fig. 1(d) would be expected. A similar checkerboard has been observed in experiments exploiting the 1-2 quantum beat, where both even and odd harmonics [26,27] have been employed. As the harmonics were energetically separated by one IR photon in these experiments, phase differences could be quantified only between different harmonics and at discrete sampling points, but not, as in our case, continuously as a function of energy and within individual harmonics. Nevertheless, these different experiments reveal similar phase variations as well.

The retrieval of the phase differences $\Delta\varphi^{\pm}_{1-2}$ from the asymmetry comprises three steps. First, we determine the modulus of the one-photon amplitude $|A^{1}_{1}(E)| = \sqrt{f^{\mathrm{XUV}}_{\mathrm{tot}}(E)}$ from an XUV-only spectrum. Second, the modulus of the two-photon amplitudes for absorption and emission $|A^{\pm}|$ are determined by fitting transition ratios to the delay-integrated RABBITT spectrum [Fig. 2(a)]. The amplitudes of the two-photon pathways are approximated as replicas of the one-photon amplitudes, shifted by the IR photon energy:

$$A^{+}(E) = r^{+}(E)A^{1}_{1}(E-\hbar\omega_{\mathrm{IR}}), \tag{6}$$

$$A^{-}(E) = r^{-}(E)A^{1}_{1}(E+\hbar\omega_{\mathrm{IR}}), \tag{7}$$

with $r^{\pm}(E) = c^{\pm} + d^{\pm}E$. The parameters $c^{\pm}$ and $d^{\pm}$ account for the smooth energy dependence of the transition ratios (see Appendix A) and are fitted to the delay-integrated RABBITT spectrum (see Appendix B),

$$\langle f_{\mathrm{tot}}(E,\tau)\rangle_{\tau} = |A^{1}(E)|^{2} + 2|A^{+}(E)|^{2} + 2|A^{-}(E)|^{2}. \tag{8}$$

Finally, using $a^{+}(E)$ and $a^{-}(E)$, we can analytically determine $\Delta\varphi^{\pm}_{1-2}(E)$ from the measured amplitude $A(E)$ and phase $\delta(E)$ of the asymmetry signal as continuous function of the energy via Eq. (5) (for the explicit solution see Appendix C). We note that for ionization from other than s-ground states, the parametrization of the angular dependent ionization amplitude must be extended to account for partial waves with different l- and m-quantum numbers. For the procedure to be consistent, the retrieved phase differences must satisfy the identity $\Delta\varphi^{+}_{1-2}(E) = \Delta\varphi^{-}_{1-2}(E-\hbar\omega_{\mathrm{IR}})$. Figure 2(c) shows that $\Delta\varphi^{+}_{1-2}(E)$ and $\Delta\varphi^{-}_{1-2}(E-\hbar\omega_{\mathrm{IR}})$ are indeed in close agreement with each other across a wide energy range, demonstrating the applicability of the phase retrieval and, in parallel, enabling a consistency check. It is important to stress that this deviation is not a statistically error estimate, nor can it be interpreted as a retrieval error. For this reason, it cannot be compared with the retrieval errors reported for other pulse retrieval or reconstruction techniques. That said, a larger deviation of the two phase differences, e.g., for the energies slightly above 6 eV and 9 eV, does indicate larger uncertainties for these energies.

V. DISCUSSION AND CONCLUSION

The retrieved phase differences from the 1-2 quantum beat method exhibit periodic oscillations with the same periodicity as the XUV harmonics, similar to those observed in the experiments employing both even and odd high harmonics [26,27]. Since in this energy region neither the EWS scattering phase nor the cc-phase of atomic helium oscillate [52–54], the phase oscillations can be attributed to the ionizing APT. To support this hypothesis, we simulate the experiment by solving the TDSE in the single-active-electron (SAE) approximation [55]. We have checked for several delay steps that a full two-electron calculation [56,57] yields indistinguishable results. As input we use an XUV pulse featuring spectral phase oscillations. As expected, we obtain an asymmetry signal exhibiting a qualitatively similar checkerboard pattern [Fig. 3(b)]. The tilt observed in the pattern is due to the attochirp of the pulse. We further verify the retrieval method by applying it to the simulated data and comparing the result to the original XUV phase. Figure 3(c) shows the excellent agreement between the phase difference $\Delta\varphi^{+,\mathrm{inp.}}_{1-2}$ from the input phase and the retrieved phase differences $\Delta\varphi^{+}_{1-2}$ and $\Delta\varphi^{-}_{1-2}$. The small deviation of the latter two across the full energy range indicates the accurate phase retrieval for all energies. The slight deviation with respect to the input phase [see Fig. 3(c)] at low kinetic energies indicates the retrieval error due to the EWS and IR-induced cc-phase [see approximations in Eq. (5)], which are no longer negligible at these energies and cannot be separated from the XUV phase by the retrieval method. The root-mean-squared deviation with respect to the input phase is 0.16 rad across the full energy range, with a maximal deviation of 0.35 rad at 4 eV.

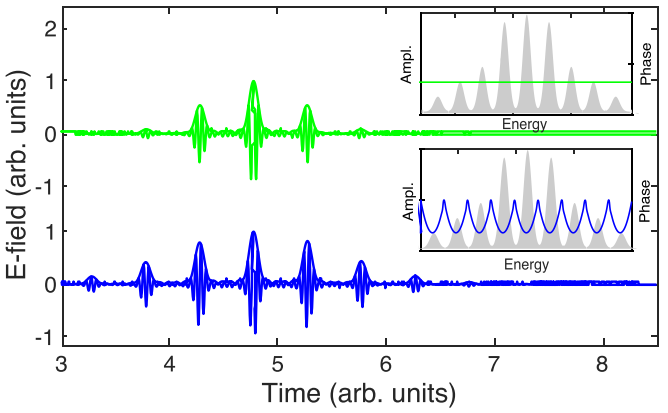

FIG. 4. Comparison of simulated attosecond pulse trains (APTs) with periodic oscillations of the spectral phase (blue) and with a flat phase (green). The spectrum is identical for both APTs. The insets show the spectrum and the corresponding phase for both APTs.

The 1-2 quantum beat method enables the measurement of phase variations across an individual harmonic. This is fundamentally different from measuring phase differences between the same spectral region of different harmonics. Therefore, this method gives us the ability to simultaneously measure the atto- and the femtochirp of the APT inherent to the HHG process [36]. The attochirp, which corresponds to a linear increase (or decrease) of the group delay across the full spectrum, is encoded in the slope of the mean of $\Delta\varphi^{\pm}_{1-2}(E)$. In the time domain, the attochirp translates into different harmonics being emitted at different times during the IR cycle stretching each attosecond burst.

The femtochirp corresponds to the observed oscillations of $\Delta\varphi^{\pm}_{1-2}(E)$. Such a rapidly varying phase within a given harmonic in the plateau region was originally predicted more than 15 years ago [36]. The femtochirp results from the interplay of two microscopic effects. First, the phase of each harmonic depends on the IR intensity at the time of tunnel ionization [58]. The use of ultrashort pulsed light sources to drive HHG implies a rapidly varying intensity envelope, which results in fine-scale phase structures within each harmonic. Second, several quantum paths contribute, in general, to the generation of the harmonics in the plateau region. Even though the intensity dependence of the phase for each path is approximately linear, the superposition of multiple paths with different phase drifts leads to a complex phase structure within each harmonic [59]. Both effects, therefore, can give rise to a femtochirp, which, in the time domain, results in an unequal spacing of the attosecond bursts [36] and stretches the envelope of the pulse train; see Fig. 4. As shown in a similar experiment [60] with a well-controlled APT of two or three attosecond bursts, the induced angular asymmetry can also be interpreted as a time-slit interference of bursts with unequal emission time, corresponding to the femtochirp. As the multi-quantum-path interference is sensitive to and easily suppressed by macroscopic propagation effects, we expect the intensity envelope effect to be the dominant contribution under realistic experimental conditions.

In conclusion, we have shown that the 1-2 quantum beat method can be used to retrieve phase variations of a photoelectron wave packet as a continuous function of energy, with a finer energy resolution than the probe frequency spectral width. In particular, we demonstrate with a proof-of-principle experiment that the 1-2 quantum beat method allows us to observe the strong periodic modulations of the spectral phase due to the harmonic chirp and caused by the HHG process itself. As the retrieval method returns phase differences as a continuous function of energy and is given in closed form, it constitutes a valuable tool to investigate also more complex photoionization dynamics and provides unprecedented access to the spectral phase of wave packets resulting from the breakup of quantum systems.

ACKNOWLEDGMENTS

All authors acknowledge the COST action CA18222 (Attosecond Chemistry). J.F., L.C., and U.K. acknowledge the support of the NCCR MUST, funded by the Swiss National Science Foundation. L.A. and N.D. acknowledge the support of the U.S. National Science Foundation under NSF Grants No. PHY-1607588 and No. PHY-1912507 and by the UCF in-house OR Grant Acc. No. 24089045. Parts of the calculations were performed on the Vienna Scientific Cluster (VSC3). S.D. and J.B. acknowledge the support by the WWTF through Project No. MA14-002, and the FWF through Projects No. FWF-SFB041-VICOM and No. FWF-W1243-Solids4Fun, as well as the IMPRS-APS. F.M. acknowledges the MICINN projects PID2019-105458RB-I00, the "Severo Ochoa" Programme for Centres of Excellence in R&D (SEV-2016-0686), and the "María de Maeztu" Programme for Units of Excellence in R&D (CEX2018-000805-M).

APPENDIX A: CHARACTERIZATION OF THE CC-TRANSITION AMPLITUDES

To characterize the cc-transition amplitudes, we compare the results of numerically calculated photoelectron spectra (PES) in helium for three different cases: (1) one narrow XUV harmonic in the absence of the IR; (2) the same XUV harmonic plus an IR field with intensity 1×10^{11} W/cm^2; and (3) the same XUV harmonic plus an IR field with intensity 2×10^{11} W/cm^2. The calculations are performed using the singe-active electron (SAE) approximation and the model potential from [48]. We have verified that full two-electron simulations give nearly identical results. Since the amplitude of the IR field is constant across a time interval wider than the APT duration, and the target does not exhibit any resonance in the spectral region of interest, the results are the same as for a purely monochromatic IR light. In particular, to the lowest perturbative order, there is no quantum path interference, and the resulting PES does not depend on the XUV-IR delay. We integrate the resulting total yield for the XUV-only simulation and the two-photon peaks for the two-color simulations. Figure 5 shows the two-color PES for an XUV energy of 35 eV and IR intensity of 2×10^{11} W/cm^2. The two-photon peaks are well separated from the one-photon peak.

The modulus of the one-photon and two-photon-amplitudes can be obtained by taking the square root of the corresponding one-photon and two-photon yields, respectively. The relative amplitudes for absorption (emission) are then calculated by dividing the higher (lower) two-photon

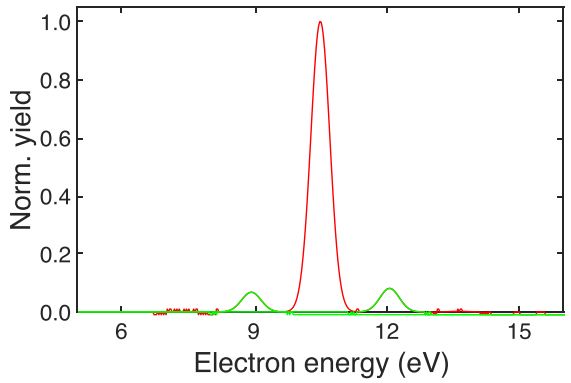

FIG. 5. (a) Photoelectron yield from the SAE simulation for helium for the two-color case with an XUV energy of 35 eV and IR intensity of 2×10^{11} W/cm^2. The side peaks (green) correspond to the two-photon transitions for additional absorption or emission of one IR photon.

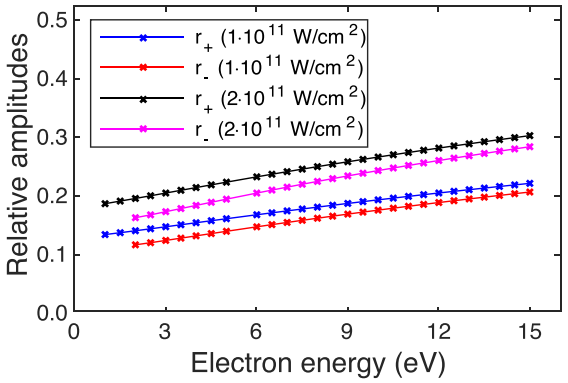

FIG. 6. Relative amplitudes for the IR induced two-photon transitions as a function of energy for additional absorption and emission of an IR photon and for different intensities of the IR field (10^{11} W/cm^2 and 2×10^{11} W/cm^2). The relative amplitudes for the higher intensity case are $\sim\sqrt{2}$ higher compared to the weak intensity case as they scale with the strength of the electric field. The energy axis refers to the electron energy of the corresponding one-photon amplitude.

amplitude by the one-photon amplitude. The calculation is repeated for all XUV energies from 24.5 eV to 40 eV in steps of 0.5 eV. Figure 6 shows the relative amplitudes as a function of the energy, justifying the assumption of linear transition ratios [Eqs. (6) and (7)].

As can be seen from the comparison between the relative amplitudes from different IR-intensities, the relative amplitudes for both absorption and emission scale with the square root of the IR intensity, in line with the fact that the two-photon amplitude is proportional to the electric field strength.

APPENDIX B: TOTAL PHOTOELECTRON YIELD

The total photoelectron signal is determined by integration of Eq. (2) over all emission angles and thus reads

$$\begin{aligned} f_{\mathrm{tot}}(E,\tau) &= \int_0^{2\pi}\int_0^{\pi} I(E,\vartheta,\tau)\sin(\vartheta)\,d\vartheta\,d\phi \\ &= |A^1(E)|^2 + \sum_{\ell=s,d}[|A_\ell^+(E)|^2 + |A_\ell^-(E)|^2 \\ &\quad + 2|A_\ell^+(E)||A_\ell^-(E)|\cos(2\omega\tau + \varphi_\ell^+ - \varphi_\ell^-)] \\ &\approx |A^1(E)|^2 + 2|A^+(E)|^2 + 2|A^-(E)|^2 \\ &\quad + 4|A^+(E)||A^-(E)|\cos(2\omega\tau + \varphi^+ - \varphi^-). \end{aligned}$$

The photoelectron spectrum corresponds to the $2\omega_{\mathrm{IR}}$-RABBITT signal. [45]. When the delay is integrated over a full IR cycle, the cosine term vanishes.

APPENDIX C: SOLUTION FOR THE IONIZATION PHASE

The modulus $A(E)$ and the phase $\delta(E)$ of the ω_{IR} oscillation amplitude are obtained via Fourier transformation of the experimental asymmetry signal. The quantities $a^+(E)$ and $a^-(E)$ [compare with Eq. (4)] are obtained by fitting the transition ratios to the integrated PES. From the two equations

$$\begin{aligned} A(E) &= |a^+ e^{i\Delta\varphi_{1-2}^+} - a^- e^{i\Delta\varphi_{1-2}^-}|, \\ \delta(E) &= \arg\,(a^+ e^{i\Delta\varphi_{1-2}^+} - a^- e^{i\Delta\varphi_{1-2}^-}), \end{aligned}$$

it is possible to retrieve $\Delta\varphi_{1-2}^{\pm}(E)$ analytically. Let $\chi = \Delta\varphi_{1-2}^- - \Delta\varphi_{1-2}^+$, then

$$A^2(E) = a^{+2} + a^{-2} - 2a^+a^-\cos\chi,$$

which can be solved for χ as

$$\chi = \pm\arccos\left(\frac{A^2 - a^{+2} - a^{+2}}{2a^+a^-}\right).$$

The correct sign determination for χ is ascertained *a posteriori* by requiring for consistency the constraint $\Delta\varphi_{1-2}^+(E) = \Delta\varphi_{1-2}^-(E - E_0)$ to be satisfied. From the value of χ and the expression for $\delta(E)$, it is straightforward to retrieve the two phases $\Delta\varphi_{1-2}^{\pm}$ as

$$\begin{aligned} \Delta\varphi_{1-2}^+ &= \delta(E) - \arg\,(a^+ - a^- e^{i\chi}), \\ \Delta\varphi_{1-2}^- &= \chi + \Delta\varphi_{1-2}^+. \end{aligned}$$

This solution holds for all energies, so that the phase differences $\Delta\varphi_{1-2}^{\pm}$ can be retrieved across the full spectrum.

[1] M. Schultze, M. Fiess, N. Karpowicz, J. Gagnon, M. Korbman, M. Hofstetter, S. Neppl, A. L. Cavalieri, Y. Komninos, T. Mercouris *et al.*, Delay in photoemission, Science **328**, 1658 (2010).

[2] M. Isinger, R. J. Squibb, D. Busto, S. Zhong, A. Harth, D. Kroon, S. Nandi, C. L. Arnold, M. Miranda, J. M. Dahlström *et al.*, Photoionization in the time and frequency domain, Science **358**, 893 (2017).

[3] C. Cirelli, C. Marante, S. Heuser, C. L. Petersson, Á. J. Galán, L. Argenti, S. Zhong, D. Busto, M. Isinger, S. Nandi *et al.*, Anisotropic photoemission time delays close to a Fano resonance, Nat. Commun. **9**, 955 (2018).

[4] G. Sansone, F. Kelkensberg, J. F. Pérez-Torres, F. Morales, M. F. Kling, W. Siu, O. Ghafur, P. Johnsson, M. Swoboda, E. Benedetti *et al.*, Electron localization following attosecond molecular photoionization, Nature (London) **465**, 763 (2010).

[5] J. Vos, L. Cattaneo, S. Patchkovskii, T. Zimmermann, C. Cirelli, M. Lucchini, A. Kheifets, A. S. Landsman, and U. Keller, Orientation-dependent stereo Wigner time delay and electron localization in a small molecule, Science **360**, 1326 (2018).

[6] A. L. Cavalieri, N. Müller, T. Uphues, V. S. Yakovlev, A. Baltuška, B. Horvath, B. Schmidt, L. Blümel, R. Holzwarth, S. Hendel *et al.*, Attosecond spectroscopy in condensed matter, Nature (London) **449**, 1029 (2007).

[7] R. Locher, L. Castiglioni, M. Lucchini, M. Greif, L. Gallmann, J. Osterwalder, M. Hengsberger, and U. Keller, Energy-dependent photoemission delays from noble metal surfaces by attosecond interferometry, Optica **2**, 405 (2015).

[8] L. Kasmi, M. Lucchini, L. Castiglioni, P. Kliuiev, J. Osterwalder, M. Hengsberger, L. Gallmann, P. Krüger, and U. Keller, Effective mass effect in attosecond electron transport, Optica **4**, 1492 (2017).

[9] M. Ossiander, J. Riemensberger, S. Neppl, M. Mittermair, M. Schäffer, A. Duensing, M. S. Wagner, R. Heider, M. Wurzer, M. Gerl *et al.*, Absolute timing of the photoelectric effect, Nature (London) **561**, 374 (2018).

[10] R. Pazourek, J. Feist, S. Nagele, and J. Burgdörfer, Attosecond Streaking of Correlated Two-Electron Transitions in Helium, Phys. Rev. Lett. **108**, 163001 (2012).

[11] C. Marante, M. Klinker, T. Kjellsson, E. Lindroth, J. González-Vázquez, L. Argenti, and F. Martín, Photoionization using the XCHEM approach: Total and partial cross sections of Ne and resonance parameters above the $2s^2 2p^5$ threshold, Phys. Rev. A **96**, 022507 (2017).

[12] Á. Jiménez-Galán, F. Martín, and L. Argenti, Two-photon finite-pulse model for resonant transitions in attosecond experiments, Phys. Rev. A **93**, 023429 (2016).

[13] V. Gruson, L. Barreau, Jiménez-Galan, F. Risoud, J. Caillat, A. Maquet, B. Carré, F. Lepetit, J. F. Hergott, T. Ruchon *et al.*, Attosecond dynamics through a Fano resonance: Monitoring the birth of a photoelectron, Science **354**, 734 (2016).

[14] M. Kotur, D. Guénot, Á. Jiménez-Galán, D. Kroon, E. W. Larsen, M. Louisy, S. Bengtsson, M. Miranda, J. Mauritsson, C. L. Arnold *et al.*, Spectral phase measurement of a Fano resonance using tunable attosecond pulses, Nat. Commun. **7**, 10566 (2016).

[15] V. Stooß, S. M. Cavaletto, S. Donsa, A. Blättermann, P. Birk, C. H. Keitel, I. Březinová, J. Burgdörfer, C. Ott, and T. Pfeifer, Real-Time Reconstruction of the Strong-Field-Driven Dipole Response, Phys. Rev. Lett. **121**, 173005 (2018).

[16] D. Polli, P. Altoè, O. Weingart, K. M. Spillane, C. Manzoni, D. Brida, G. Tomasello, G. Orlandi, P. Kukura, R. A. Mathies *et al.*, Conical intersection dynamics of the primary photoisomerization event in vision, Nature (London) **467**, 440 (2010).

[17] J. Itatani, F. Quéré, G. L. Yudin, M. Y. Ivanov, F. Krausz, and P. B. Corkum, Attosecond Streak Camera, Phys. Rev. Lett. **88**, 173903 (2002).

[18] M. Ossiander, F. Siegrist, V. Shirvanyan, R. Pazourek, A. Sommer, T. Latka, A. Guggenmos, S. Nagele, J. Feist, J. Burgdörfer *et al.*, Attosecond correlation dynamics, Nat. Phys. **13**, 280 (2017).

[19] P. M. Paul, E. S. Toma, P. Breger, G. Mullot, F. Auge, P. Balcou, H. G. Muller, and P. Agostini, Observation of a train of attosecond pulses from high harmonic generation, Science **292**, 1689 (2001).

[20] H. Muller, Reconstruction of attosecond harmonic beating by interference of two-photon transitions, Appl. Phys. B **74**, s17 (2002).

[21] Y. Mairesse and F. Quéré, Frequency-resolved optical gating for complete reconstruction of attosecond bursts, Phys. Rev. A **71**, 011401(R) (2005).

[22] M. Chini, S. Gilbertson, S. D. Khan, and Z. Chang, Characterizing ultrabroadband attosecond lasers, Opt. Express **18**, 13006 (2010).

[23] D. Busto, L. Barreau, M. Isinger, M. Turconi, C. Alexandridi, A. Harth, S. Zhong, R. J. Squibb, D. Kroon, S. Plogmaker *et al.*, Time–frequency representation of autoionization dynamics in helium, J. Phys. B **51**, 044002 (2018).

[24] L. Barreau, C. L. Petersson, M. Klinker, A. Camper, C. Marante, T. Gorman, D. Kiesewetter, L. Argenti, P. Agostini, J. González-Vázquez *et al.*, Disentangling Spectral Phases of Interfering Autoionizing States from Attosecond Interferometric Measurements, Phys. Rev. Lett. **122**, 253203 (2019).

[25] S. Donsa, N. Douguet, J. Burgdörfer, I. Březinová, and L. Argenti, Circular Holographic Ionization-Phase Meter, Phys. Rev. Lett. **123**, 133203 (2019).

[26] G. Laurent, W. Cao, H. Li, Z. Wang, I. Ben-Itzhak, and C. L. Cocke, Attosecond Control of Orbital Parity Mix Interferences and the Relative Phase of Even and Odd Harmonics in an Attosecond Pulse Train, Phys. Rev. Lett. **109**, 083001 (2012).

[27] G. Laurent, W. Cao, I. Ben-Itzhak, and C. L. Cocke, Attosecond pulse characterization, Opt. Express **21**, 16914 (2013).

[28] V. Loriot, A. Marciniak, G. Karras, B. Schindler, G. Renois-Predelus, I. Compagnon, B. Concina, R. Brédy, G. Celep, C. Bordas *et al.*, Angularly resolved RABBITT using a second harmonic pulse, J. Opt. **19**, 114003 (2017).

[29] V. Loriot, A. Marciniak, S. Nandi, G. Karras, M. Hervé, E. Constant, E. Plésiat, A. Palacios, F. Martín, and F. Lépine, High harmonic generation-2ω attosecond stereo-photoionization interferometry in N_2, J. Phys. Photonics **2**, 024003 (2020).

[30] H. J. Shin, D. G. Lee, Y. H. Cha, K. H. Hong, and C. H. Nam, Generation of Nonadiabatic Blueshift of High Harmonics in an Intense Femtosecond Laser Field, Phys. Rev. Lett. **83**, 2544 (1999).

[31] H. J. Shin, D. G. Lee, Y. H. Cha, J. H. Kim, K. H. Hong, and C. H. Nam, Nonadiabatic blueshift of high-order harmonics from Ar and Ne atoms in an intense femtosecond laser field, Phys. Rev. A **63**, 053407 (2001).

[32] Y. Mairesse, O. Gobert, P. Breger, H. Merdji, P. Meynadier, P. Monchicourt, M. Perdrix, P. Salières, and B. Carré, High Harmonic XUV Spectral Phase Interferometry for Direct Electric-Field Reconstruction, Phys. Rev. Lett. **94**, 173903 (2005).

[33] S. Haessler, L. B. Bom, O. Gobert, J. F. Hergott, F. Lepetit, M. Perdrix, B. Carré, T. Ozaki, and P. Salières, Femtosecond envelope of the high-harmonic emission from ablation plasmas, J. Phys. B **45**, 074012 (2012).

[34] F. Ardana-Lamas, C. Erny, A. G. Stepanov, I. Gorgisyan, P. Juranić, R. Abela, and C. P. Hauri, Temporal characterization of individual harmonics of an attosecond pulse train by THz streaking, Phys. Rev. A **93**, 043838 (2016).

[35] K. T. Kim, C. Zhang, T. Ruchon, J. F. Hergott, T. Auguste, D. M. Villeneuve, P. B. Corkum, and F. Quéré, Photonic streaking of attosecond pulse trains, Nat. Photonics **7**, 651 (2013).

[36] K. Varjú, Y. Mairesse, B. Carré, M. B. Gaarde, P. Johnsson, S. Kazamias, R. López-Martens, J. Mauritsson, K. J. Schafer, P. Balcou *et al.*, Frequency chirp of harmonic and attosecond pulses, J. Mod. Opt. **52**, 379 (2005).

[37] J. Mauritsson, P. Johnsson, R. López-Martens, K. Varjú, W. Kornelis, J. Biegert, U. Keller, M. B. Gaarde, K. J. Schafer, and A. L'Huillier, Measurement and control of the frequency chirp rate of high-order harmonic pulses, Phys. Rev. A **70**, 021801(R) (2004).

[38] K. T. Kim, D. H. Ko, J. Park, V. Tosa, and C. H. Nam, Complete temporal reconstruction of attosecond high-harmonic pulse trains, New J. Phys. **12**, 083019 (2010).

[39] E. P. Wigner, Lower limit for the energy derivative of the scattering phase shift, Phys. Rev. **98**, 145 (1955).

[40] F. T. Smith, Lifetime matrix in collision theory, Phys. Rev. **118**, 349 (1960).

[41] S. Nagele, R. Pazourek, J. Feist, K. Doblhoff-Dier, C. Lemell, K. Tőkési, and J. Burgdörfer, Time-resolved photoemission by attosecond streaking: Extraction of time information, J. Phys. B **44**, 081001 (2011).

[42] K. Klünder, J. M. Dahlström, M. Gisselbrecht, T. Fordell, M. Swoboda, D. Guénot, P. Johnsson, J. Caillat, J. Mauritsson, A. Maquet *et al.*, Probing Single-Photon Ionization on the Attosecond Time Scale, Phys. Rev. Lett. **106**, 143002 (2011).

[43] Y. Mairesse, D. de Bohan, L. J. Frasinski, H. Merdji, L. C. Dinu, P. Monchicourt, P. Breger, M. Kovacev, R. Taieb, B. Carre *et al.*, Attosecond synchronization of high-harmonic soft X-rays, Science **302**, 1540 (2003).

[44] V. Véniard, R. Taïeb, and A. Maquet, Phase dependence of $(N+1)$-color $(N>1)$ ir-uv photoionization of atoms with higher harmonics, Phys. Rev. A **54**, 721 (1996).

[45] J. M. Dahlström, D. Guénot, K. Klünder, M. Gisselbrecht, J. Mauritsson, A. L'Huillier, A. Maquet, and R. Taïeb, Theory of attosecond delays in laser-assisted photoionization, Chem. Phys. **414**, 53 (2013).

[46] J. Fuchs, N. Douguet, S. Donsa, F. Martin, J. Burgdörfer, L. Argenti, L. Cattaneo, and U. Keller, Time delays from one-photon transitions in the continuum, Optica **7**, 154 (2020).

[47] D. Busto, J. Vinbladh, S. Zhong, M. Isinger, S. Nandi, S. Maclot, P. Johnsson, M. Gisselbrecht, A. L'Huillier, E. Lindroth, and J. M. Dahlström, Fano's Propensity Rule in Angle-Resolved Attosecond Pump-Probe Photoionization, Phys. Rev. Lett. **123**, 133201 (2019).

[48] X. M. Tong and C. D. Lin, Empirical formula for static field ionization rates of atoms and molecules by lasers in the barrier-suppression regime, J. Phys. B **38**, 2593 (2005).

[49] R. Dörner, V. Mergel, O. Jagutzki, L. Spielberger, J. Ullrich, R. Moshammer, and H. Schmidt-Böcking, Cold target recoil ion momentum spectroscopy: A 'momentum microscope' to view atomic collision dynamics, Phys. Rep. **330**, 95 (2000).

[50] S. Heuser, Á. Jiménez Galán, C. Cirelli, C. Marante, M. Sabbar, R. Boge, M. Lucchini, L. Gallmann, I. Ivanov, A. S. Kheifets *et al.*, Angular dependence of photoemission time delay in helium, Phys. Rev. A **94**, 063409 (2016).

[51] M. Sabbar, S. Heuser, R. Boge, M. Lucchini, L. Gallmann, C. Cirelli, and U. Keller, Combining attosecond XUV pulses with coincidence spectroscopy, Rev. Sci. Instrum. **85**, 103113 (2014).

[52] J. Mauritsson, M. B. Gaarde, and K. J. Schafer, Accessing properties of electron wave packets generated by attosecond pulse trains through time-dependent calculations, Phys. Rev. A **72**, 013401 (2005).

[53] D. Guénot, D. Kroon, E. Balogh, E. W. Larsen, M. Kotur, M. Miranda, T. Fordell, P. Johnsson, J. Mauritsson, M. Gisselbrecht *et al.*, Measurements of relative photoemission time delays in noble gas atoms, J. Phys. B **47**, 245602 (2014).

[54] C. Palatchi, J. M. Dahlström, A. S. Kheifets, I. A. Ivanov, D. M. Canaday, P. Agostini, and L. F. Dimauro, Atomic delay in helium, neon, argon and krypton, J. Phys. B At. Mol. Opt. Phys. **47**, 245003 (2014).

[55] N. Douguet, A. N. Grum-Grzhimailo, E. V. Gryzlova, E. I. Staroselskaya, J. Venzke, and K. Bartschat, Photoelectron angular distributions in bichromatic atomic ionization induced by circularly polarized VUV femtosecond pulses, Phys. Rev. A **93**, 033402 (2016).

[56] J. Feist, S. Nagele, R. Pazourek, E. Persson, B. I. Schneider, L. A. Collins, and J. Burgdörfer, Nonsequential two-photon double ionization of helium, Phys. Rev. A **77**, 043420 (2008).

[57] S. Donsa, I. Březinová, H. Ni, J. Feist, and J. Burgdörfer, Polarization tagging of two-photon double ionization by elliptically polarized XUV pulses, Phys. Rev. A **99**, 023413 (2019).

[58] M. Lewenstein, P. Salières, and A. L'Huillier, Phase of the atomic polarization in high-order harmonic generation, Phys. Rev. A **52**, 4747 (1995).

[59] M. B. Gaarde and K. J. Schafer, Quantum path distributions for high-order harmonics in rare gas atoms, Phys. Rev. A **65**, 031406(R) (2002).

[60] Y.-C. Cheng, S. Mikaelsson, S. Nandi, L. Rämisch, C. Guo, S. Carlström, A. Harth, J. Vogelsang, M. Miranda, C. L. Arnold *et al.*, Controlling photoionization using attosecond time-slit interferences, Proc. Natl. Acad. Sci. USA **117**, 10727 (2020).